Molecular Crystals and Liquid Crystals
Publication details, including instructions for authors and subscription information:
http://www.tandfonline.com/loi/gmcl16

Structure, Phase Diagram and Fluorescence Spectra of 2,3-Dimethylnaphthalene (Anthracene) Mixed Crystals

Norbert Karl [a] , Hans Heym [a] & John J. Stezowski [b]
[a] Physikalisches Institut - Teil 3 der Universität Stuttgart, Pfaffenwaldring, 57, D 7000, Stuttgart-80, Federal Republic of Germany
[b] Institut für Organische Chemie, Biochemie and Isotopenforschung der Universität Stuttgart, Pfaffenwaldring, 55, D 7000, Stuttgart-80, Federal Republic of Germany
Version of record first published: 20 Apr 2011.

To cite this article: Norbert Karl , Hans Heym & John J. Stezowski (1985): Structure, Phase Diagram and Fluorescence Spectra of 2,3-Dimethylnaphthalene (Anthracene) Mixed Crystals, Molecular Crystals and Liquid Crystals, 131:1-2, 163-191

To link to this article: http://dx.doi.org/10.1080/00268948508084200

Mol. Cryst. Liq. Cryst., 1985, Vol. 131, pp. 163–192
0026-8941/85/1312–0163/$25.00/0

Structure, Phase Diagram and Fluorescence Spectra of 2,3-Dimethylnaphthalene (Anthracene) Mixed Crystals

NORBERT KARL, HANS HEYM

Physikalisches Institut - Teil 3 der Universität Stuttgart, Pfaffenwaldring 57, D 7000 Stuttgart-80, Federal Republic of Germany

and

JOHN J. STEZOWSKI

Institut für Organische Chemie, Biochemie and Isotopenforschung der Universität Stuttgart, Pfaffenwaldring 55, D 7000 Stuttgart-80, Federal Republic of Germany

(*Received Feburary 7, 1985*)

An X-ray *crystal structure determination* for 2,3-dimethylnaphthalene (2,3-DMN) at 300 K was carried out. The two noncentrosymmetric molecules in the unit cell, space group $P2_1/a$, (a = 7.916(10) Å, b = 6.052(8) Å, c = 10.017(8) Å, β = 105.43(1)°) are statistically dipolarly disordered. Perfect cleavage along (001) is examined in terms of the disordered structure. There are two phase transitions, one of higher order from monoclinic to triclinic, occuring at ~210K, and another one at ~100K. The *phase diagram* of 2,3-DMN/anthracene exhibits a peritectic at 377.4K (104.2°C) with continuous mixed crystal formation from 0 to ~23% anthracene (confirmed by X-ray Guinier technique). From normal freezing experiments a concentration-dependent distribution coefficient k of anthracene (A) in 2,3-DMN is derived with $k(c_A \rightarrow 0)$ = 2.16. Packing of the mixed crystals is analyzed in terms of lattice geometry and packing coefficients. Liq. He *fluorescence and absorption spectra* of anthracene in 2,3-DMN display a fairly large residual line width, $\Delta \sim 300\ cm^{-1}$ which is attributed to the statistical disorder of the host lattice. Spectral changes of the anthracene guest fluorescence emission observed with increasing anthracene concentration are taken to be indicative of guest-guest interactions.

I. INTRODUCTION

This work was initiated by the need for mixed crystal systems with a wide range of miscibility, suitable for fundamental investigations of

energy and charge transport in van der Waals-bonded organic molecular crystals. In these systems either scattering or localization of mobile (excited) states at guest sites, or "band amalgamation" of host and guest levels can occur. Interesting problems arise from the possibility of guest-guest interactions, dimer and aggregate formation, and possible impurity band conduction at the higher guest concentrations.

In the search for useful systems our attention was drawn to 2,3-dimethylnaphthalene/anthracene, (2,3-DMN/A), a system which on the one hand was found to display mixed crystal formation (or "substitutional disorder") for anthracene concentrations from 0 to 23%, and on the other hand displayed an additional interesting aspect, that of orientational disorder (of one degree of freedom) in the 2,3-DMN host lattice.

Energy and charge transport in organic molecular crystals have been studied intensively for many years.[1,2] Considerable knowledge has been gained about excitonic energy transport and (electron and hole) charge transport in *ordered one-component crystals*, see e.g. refs.,[3-6] and,[2,7] respectively. Nevertheless, several important basic questions such as that of coherence or incoherence of the transport states have remained essentially unanswered. Transport in *orientationally disordered* one-component crystals has not yet received very much attention.

For *two-component systems* research has been concentrating on a few isotopically mixed crystals such as benzene-h_6/benzene-d_6,[8b] 1,2,4,5-tetrachlorobenzene-h_2/1,2,4,5-tetrachlorobenzene-d_2,[8t] naphthalene-h_8/naphthalene-d_8,[8n] 1,4-dibromonophthalene-h_6/1,4-dibromonaphthalene-d_6,[8d] anthracene-h_{10}/anthracene-d_{10},[8a] and phenazine-h_8/phenazine-d_8,[8p] because this special class of materials exhibits the exceptional property of forming a continuous series of ideal mixed crystals all across the binary phase diagram. The physical properties of the isotopic components, however are very similar. Nonetheless a number of basic questions on interactions and energy transfer could be clarified, but others remained open.

The search for suitable non-isotopic mixed crystals (i.e. crystals composed of chemically different molecules), with miscibility over a wide concentration range, is basically an old problem (cf. Kitaigorodsky[9]). But to date only a few systems with a miscibility greater than 0.1 . . . 1% have been found. There exist only a few investigations which were devoted to partial aspects of energy transfer see e.g.,[10-12] exciton—exciton interactions[49] and charge transport[13] in non-isotopically mixed crystals.

A wide range of miscibility is not the only criterion for a desirable

model system. Favourable optical properties such as absorption in the visible or near UV, fluorescence emission from both, host and guest molecules, and the possibility of growing large, perfect (mixed) single crystals, are other criteria. Last, but not least, ultrapurity, as is well known, is the prime condition for obtaining meaningful transport results. Transport in less pure material is usually governed by trapping and detrapping kinetics; the intrinsic transport propertites of the neat crystal are then obscured by ("extrinsic") influences from impurities (of mostly unknown nature). Therefore there was clearly a primary need for further model systems combining the property of a wide range of miscibility of the chemically different components with the possibilities of ultrapurification and the growth of large perfect (mixed) single crystals, as well as with the presence of favourable optical properties.

SEARCH FOR SUITABLE SYSTEMS AND OUTLINE OF THE PAPER

The key to understanding the poor miscibility in the crystalline state exhibited by most organic molecular systems is recognition of the great variety (of size, shape and symmetry) of organic molecular structures. Since van der Waals forces are rather unspecific, the dominant mechanism to minimize lattice free energy is the tendency to fill space by establishing as many atom-atom contacts as possible.[9] If this tendency is hindered in binary systems because of steric incompatibility of the components, the coexistence of the component lattices is very often energetically favoured over the formation of a mixed crystal lattice. It is characteristic of the simplest kind of such systems that a melting point depression occurs at both ends of the phase diagram, with the formation of a eutectic somewhere in between, and that the distribution (or "segregation") coefficient k, defined as the ratio of the dopant concentrations in the solidifying material c_s and the melt c_ℓ, $k = c_s/c_\ell$, are smaller than unity everywhere in the phase diagram.

A binary system with complete miscibility in the solid state is usually distinguished by the fact that a distribution coefficient $k > 1$ occurs at the lower melting point end of the phase diagram. Therefore, in searching for mixed crystals with a large miscibility range, we took into consideration systems with small lattice misfit factors† and ex-

†The lattice misfit factor is defined as the ratio of non overlapping to overlapping molecular volume fractions of the two different species under consideration when they are geometrically superimposed.[14]

amined (by multipass zone refining of binary mixtures at both ends of the phase diagram) if a $k > 1$ situation occurred in which the dopant concentrates at the zone entrance of the zone refining bar.

In fact in 2,3-dimethylnaphthalene, DMN, the "natural" impurity anthracene, A, displayed such behaviour; similar properties were also predicted and indeed found for the next higher homologous system tetracene in 2,3-dimethylanthracene, DMA,[15,44] and for tetracene in p-terphenyl and brazany,[16,44] respectively, compounds which also resemble the tetracene molecule geometrically.

This report describes our study of the 2,3-DMN (anthracene) system, i.e. the 2,3-DMN-rich part of the 2,3-DMN/anthracene phase diagram.

There are several favourable features displayed by this system: The optical and electrical properties of anthracene have been widely studied.[2,17] Charge carrier mobility results for purified 2,3-DMN crystals have been reported.[18] Weakly anthracene-doped crystals were investigated spectroscopically,[19] and room temperature laser emission was obtained from cleaved platelets of such (doped) samples.[20]

High purity can be obtained for both components, see e.g.,[21] and 2,3-DMN Bridgman crystals exhibit extremely good (001) cleavage giving rise to optical qualtiy surfaces; Fabry-Perot interferences can be obtained from cleaved platelets.[44] In contrast to many other organic crystals, 2,3-DMN is rather stiff and shows no propensity towards physical deformation by lattice slippage. Mosaic width, determined by X-ray rocking curves,[22] was smaller than the experimental angular resolution (0.06°). The existence of dislocation-free sections (1 cm^2) has been demonstrated by X-ray topography.[23,44]

Because the crystal structure of 2,3-DMN was unknown, we present an X-ray structure determination, followed by a description of the 2,3-DMN-rich side of the phase diagram established by thermal analysis and further characterized by precise determination of the gradual changes of the lattice parameters in a series of mixed crystals. The structural data, which include dipolar disorder in the 2,3-DMN lattice, help to understand the observed wide range of miscibility (up to ~23% anthracene). Finally, preliminary results of concentration-dependent fluorescence spectra indicate that increasing guest-guest interactions with increasing anthracene concentration lead to anthracene-crystal like spectra when the anthracene concentration exceeds ~4%.

II. EXPERIMENTAL

2,3-Dimethylnaphthalene was purified by vacuum sublimation and subsequent multipass zone refining.[21] In some cases a chemical pre-

purification by Diels Alder reaction with maleic anhydride was carried out.[21] Anthracene, scintillation grade, was vacuum sublimed and zone-refined.[21]

Single crystals of 2,3-DMN were grown either by unidirectional cooling from the melt after Bridgman-Stockbarger[21] (under vacuum and at a rate of 0.4 – 0.65 mm/h), by "Plate Sublimation" (also under vacuum),[21] or from solution by slow evaporation of the solvent. Normal Freezing was performed on a separate apparatus,[24] using samples of 3 g of material, sealed under 500 torr N_2 into glass tubes, 20 cm long and with a bore of 6.5 mm. The molten part was held a few degrees above the melting point; unidirectional solidification was achieved by moving a cooling jacket (held at 50°C) across the length of the ampoule with a speed of 3 mm/h. Thorough mixing of the melt was accomplished by inertial stirring: the ampoule, fixed in space, was rotated clockwise for 30 sec at 250 revolutions per minute, stopped for 2 sec, rotated counterclockwise, etc. .

Crystals prepared by two different methods were used for the X-ray structure determination: One of size ~0.5 x 0.5 x 0.5 mm^3 obtained from a large Bridgman crystal by cutting with a solvent saw, using a very thin thread and xylene as a solvent; the other, obtained from solution, was used untreated and had dimensions ~0.2 x 0.3 x 0.5 mm^3. The results obtained with both samples were essentially the same; so we confine ourselves to describing the analysis of the solution-grown crystal.

Intensity data were measured with a Syntex $P\bar{1}$ autodiffractometer using MoK_α (monochromatized, $\lambda = 0.71069$ Å) radiation and operating in a variable speed (2.0 – 24.0 deg s^{-1}) ω-scan mode; the scan range was 1.0 deg. Background radiation was measure on each side ($\Delta\omega = 1.0$ deg) of a reflection for one half the scan time. A total of 1032 unique reflections ($\sin(\theta/\lambda)_{max} = 0.647$ Å^{-1}) were measured of which only 264 reflections had $I \geq 3\sigma(I)$; the latter were classified as objectively observed.‡

A number of 2,3-DMN (anthracene) mixed crystals were obtained from the melt with different amounts of anthracene added (Bridgman method). These crystals were approximately 3.5–4 cm long. They were cut with a thread saw into 5 mm thick slices. The average distribution function of the anthracene dopant was obtained by gas chromatographic (GC) analysis; the components were separated on

‡The list of calculated and observed structure factors can be obtained under the full reference of this article plus CSD - number 51510 from: Fachinformationszentrum Energie, Physik, Mathematik GMBH, Fachabteilung III Daten und Fakten, D 7514 Eggenstein-Leopoldshafen 2, Fed. Rep. of Germany.

1 m × 1/8″ stainless steel columns filled with 5% XE 60 on Chromosorb W and detected with a flame ionization detector. For the analysis of cross sections of the normal freezing ingots, the samples were prepared by dissolution in benzene (after removal of an outer jacket of the slices). Using this method, the statistical error between subsequent injections amounted to a few percent. The carrier gas was nitrogen, 5N, at a flow rate of 25 ml/min.

Because only several micrograms of substance are required, solid sample injection[25] was superior for assessing the homogeneity of the normal freezing distribution or the local concentration at spots where fluorescence was probed. However, the statistical fluctuations (~10%) were greater with this method. Column temperature was 130°C for liquid injection and 160° for solid sample injection.

Distribution coefficients were calculated[26] using the average concentration function obtained as described above. However, the determination of the phase diagram by DTA, and of the relationship between composition and precise lattice constants of the mixed crystals required individual analysis of small samples (1–10 mg); solid sample injection-GC technique was also used in these cases.

One important advantage of GC-analysis is the fact that the eventual presence of other impurities (such as a very persistent fluorene impurity) is detected simultaneously. A sensitivity of 10^{-6} mol/mol can be achieved.

Thermal analysis was performed by differential thermal analysis, DTA, (Linseie L 62), generally with a heating rate of 1°/min. The temperature scale was calibrated with In and Sn. Because of high vapour pressure, samples had to be sealed into small glass tubes. Al_2O_3 was used as an inert reference substance.

The evaluation of DTA curves is somewhat ambiguous because the theoretical curve shape can only be given approximately. For sharp transitions we used the intersection point of the tangent to the rising part of the melt peak with the base line, whereas in a melting interval situation the beginning of the rise was used. The end-temperature was considered to be indicated by the intersection of the rising and the falling tangent, both drawn through the corresponding inflection point.[27]

The range of miscibility was probed by checking the continuity of lattice parameter variations by using the Guinier X-ray diffraction powder pattern technique (Irdab XDC-700 camera; monochromatized Cu-$K_{\alpha 1}$ radiation). In view of the ambiguity of several results in the literature concerning the actual miscibility ranges of other systems, this independent determination was deemed very important.

Optical fluorescence spectra were registered with a 1 m spectrograph in Czerny Turner mount (Jarrell Ash) at temperatures below the λ-point of liquid helium ($T < 2.2$ K). The fluorescence was excited with $\lambda = 280$ nm, FWHM = 40 nm from a mercury arc (HBO 200, Osram) in combination with interference reflection filters (Schott). Absorption spectra were measured on a UV/VIS spectrophotometer (Sp 8-250, Pye Unicam) equipped with a variable temperature He cryostat.

III. RESULTS OF THE X-RAY STRUCTURE DETERMINATION

Monoclinic symmetry was inferred from polarization-optical interference patterns obtained with white and monochromatic convergent light through the cleavage plane and confirmed by X-ray diffraction pattern symmetry. By refinement[28] of 26 selected automatically centered X-ray reflections the following lattice parameters of 2,3-DMN were obtained ($T = 297$ K):

$$a = 7.916(10)\ \text{Å}$$

$$b = 6.052(8)\ \text{Å}$$

$$c = 10.017(8)\ \text{Å}$$

$$\beta = 105.43(10)^\circ$$

$$V_o = 462.6\ \text{Å}^3$$

The cleavage plane is (001) from crystal optics.[29] Systematic absences of the X-ray reflections ($h0\ell$) for h odd and (0k0) for k odd uniquely inferred space group $P2_1/a$ with $Z = 2$, $\rho_{calc.} = 1.15$ g/cm^3, which requires that the molecules sit on a center of symmetry. Because the 2,3-DMN molecule is acentric, the presence of "dipolar disorder," i.e. statistical up and down orientation of the dipolar molecule, was assumed and subsequently confirmed during the structure determination.

Analysis of redundant, intramolecular vectors in an origin-removed sharpened Patterson map revealed both the orientation and position of the DMN molecules in the unit cell.

Refinement of individual atomic positions yielded an $R = 0.124$ (unit weighted) but produced a chemically unreasonable model molecular structure, which is not uncommon with disordered structures.

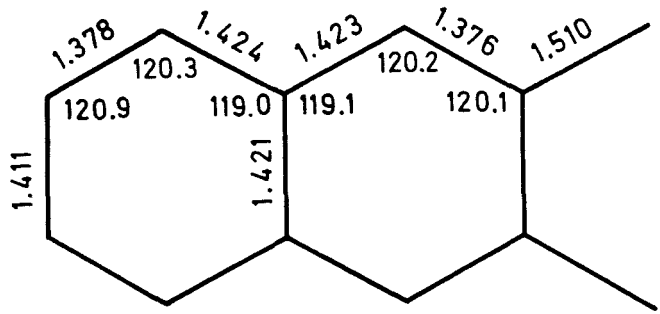

FIGURE 1 Bonding geometry of the 2,3-dimethylnaphthalene molecule, based on the naphthalene framework, taken from the literature;[39] the two methyl groups were calculated from known geometrical considerations.

Consequently, rigid body refinement was used, based on the known naphthalene molecular structure,[39] on which CH_3-groups were placed 1.510 Å from the appropriate ring C-atoms (C_2 and C_3 in Figure 2) with exocyclic angles of 120° (Figure 1). Subsequent least squares refinement of the position and orientation of the rigid body, followed by the refinement of anisotropic temperature factors with fixed coordinates, resulted in an R-value of 0.153.

A subsequent free refinement of the coordinates once again resulted in gross distortion of the molecular geometry.

Finally, we tried to ascertain if the refinement, yielding a relative displacement of 1.45 Å of the naphthalene frameworks of the two symmetry-related molecules, did not result from a local minimum. The shift was increased and decreased in steps of 0.1 Å but no lower R value was found.

The fractional atomic coordinates and the anistropic temperature factors of the room temperature monoclinic phase are reproduced in Table 1.

The molecules lie on the plane

$$0{,}886x - 0{,}460y + 0{,}058z = 0$$

where $x \| a$, $y \| b \|$ and $z \| c^*$. Their average long axis is nearly perpendicular to the (001) cleavage plane, which confirms the conclusions drawn from analysis of IR spectra and of anisotropy of the diamagnetic susceptibility and refractive index.[30] The (average) electron density in the molecular plane is plotted in Figure 2 together with the frameworks of the two disordered molecules.

A packing diagram, viewed along [010] of the unit cell, is reproduced in Figure 3. For clarity only one of the two statistically occurring

TABLE 1

Fractional atomic coordinates and anistropic temperature factors of the room temperature 2,3-DMN crystal structure for one of the two statistically occurring orientations of the 2,3-DMN molecule; the (the coordinates of the other orientation are obtained by inversion at [000]).

ATOM	x/a	y/b	z/c	U	U11	U22	U33	U12	U13	U23
C 1	.0975	.2058	.0613		.0653	.0646	.0945	.0068	.0229	.0074
C 2	.0852	.0999	.1799		.0527	.0714	.1187	−.0005	.0117	−.0272
C 3	.0011	−.1071	.1717		.0482	.0712	.1059	.0029	.0228	.0061
C 4	−.0703	−.2061	.0454		.0538	.0565	.1339	−.0010	.0144	−.0123
C 5	−.0603	−.0999	−.0791		.0470	.0531	.1282	.0063	.0249	.0049
C 6	−.1334	−.1970	−.2113		.0596	.0705	.1279	.0009	.0252	−.0235
C 7	−.1211	−.0911	−.3300		.1164	.1549	.0817	.0068	.0210	−.0222
C 8	−.0370	.1160	−.3217		.1030	.1392	.0907	.0129	.0194	−.0054
C 9	.0344	.2149	−.1953		.0583	.0845	.1128	.0080	.0307	−.0055
C10	.0245	.1087	−.0708		.0521	.0640	.0677	.0025	.0223	.0024
C11	.1619	.2058	.3195		.1107	.1158	.0836	−.0091	.0224	−.0172
C12	−.0107	−.2216	.3028		.1048	.1012	.0778	.0009	.0316	.0068
H(C1)	.1631	.3636	.0685	.2742						
H(C4)	−.1340	−.3648	.0407	.3107						
H(C6)	−.1990	−.3548	−.2185	.1366						
H(C7)	−.1759	−.1668	−.4297	.1230						
H(C8)	−.0286	.1979	−.4154	.0816						
H(C9)	.0981	.3736	−.1907	.0934						

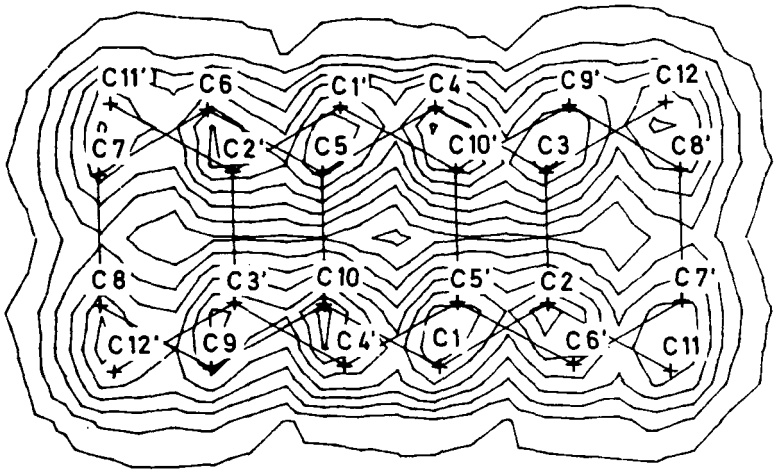

FIGURE 2 Electron density contoured at 1e/Å^3 levels[38] in the plane of the 2,3-DMN molecule.

molecular orientations on the lattice sites is shown. The other orientation (for which the atomic coordinates are given in Table 7) is obtained by inversion of the molecule at [000] etc.

Collecting a low temperature data set, which could provide more information, was attempted, but not pursued, because upon cooling a single crystal many reflections showed splitting. This precluded measurement of meaningful intensity data. The splitting was taken as a probable indication of twinning, but could have resulted from crystal strain.

A Guinier powder photograph at continuously decreasing temperature[31] indicated two phase transitions, one at ~210 K, the other at ~100 K. From an analysis of the Guinier powder data it was found that the equivalence in monoclinic symmetry of the two sets of reflections $2\theta_{\pm(hk\ell)}$ and $2\theta_{\pm(h\bar{k}\ell)}$ gradually disappears at about 210 K, leading to a splitting of the reflections $2\theta_{(hk\ell)}$ and $2\theta_{(h\bar{k}\ell)}$ for $k \geq 1$ and $|h| + |\ell| \neq 0$, which is indicative of a (higher order) phase transition from monoclinic to triclinic symmetry.

The second phase transition occurring at ~100 K has also been observed in laser emission spectroscopy;[45] from hysteresis a first order transition has been inferred.[46]

IV. RESULTS OF THE THERMAL AND GUINIER PHASE DIAGRAM ANALYSIS FOR THE MIXED 2,3-DMN/A SYSTEM

The temperature points obtained for the liquidus and solidus curves by DTA are plotted in Figure 4 for the 2,3-DMN-rich side of the

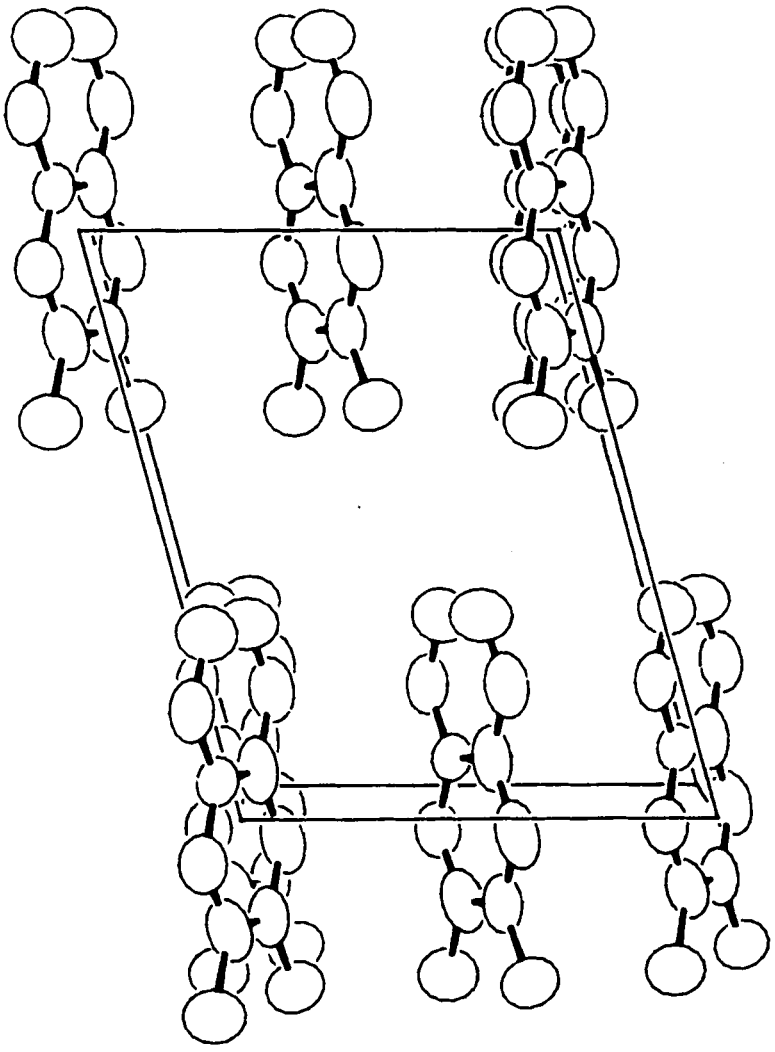

FIGURE 3 The unit cell of 2,3-DMN, viewed along the b-direction; (a is horizontal, the origin is at the front lower left corner). For clarity the 2,3-DMN molecules are plotted for only one of the two statistically occurring orientations and two molecules have been omitted, one at [100] and one at [077].

phase diagram where anthracene can be considered as the dopant. (The absolute temperature accuracy is approximately ± 1 deg; the melting points of anthracene and 2,3-DMN were determined at 215.9 and 104.2° C, respectively.) There is a peritectic point at 113° C for a concentration of ~86% 2,3-DMN in the melt. The distribution

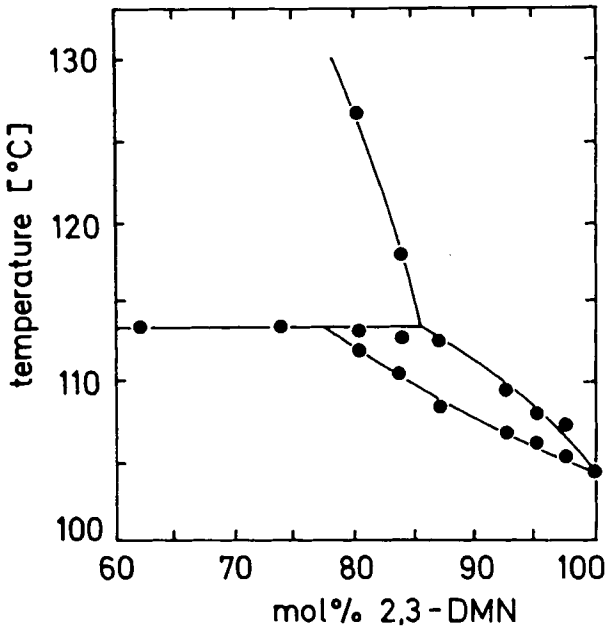

FIGURE 4 2,3-DMN-rich side of the phase diagram 2,3-DMN(anthracene), as obtained by DTA.

coefficient k for anthracene is greater than 1; mixed crystals are formed between 0 and ~23% anthracene.

The other end of the phase diagram was not studied in much detail. The solid state miscibility range is from 0 to between 10 and 20%. For 21% 2,3-DMN inhomogeneous peritectic melting at 113° C was observed. The phase diagram resembles those of the dibenzofuran-anthracene[32] and of the brazan-tetracene[44] systems.

Continuous miscibility was confirmed by X-ray powder methods (Guinier technique) for mixed crystals containing between 0 and 20 mol-% anthracene. The lattice parameters changed continuously in this concentration range, see Figure 5. The relative accuracy of the interplanar distances, d_{hkl}, is ~0.01 Å (at 5 Å).

The distribution coefficient of anthracene between liquid and crystalline 2,3-DMN in mixtures containing different anthracene concentrations was determined from bars prepared by unidirectional cooling (Normal Freezing). The bars were cut into 1 cm sections from which 1 mm slices were taken for analysis by GC.

For a normal freezing situation under real conditions we must take into account that on cooling successive parts of the solidified material crack off from the ampoule wall as the ingot contracts, resulting in

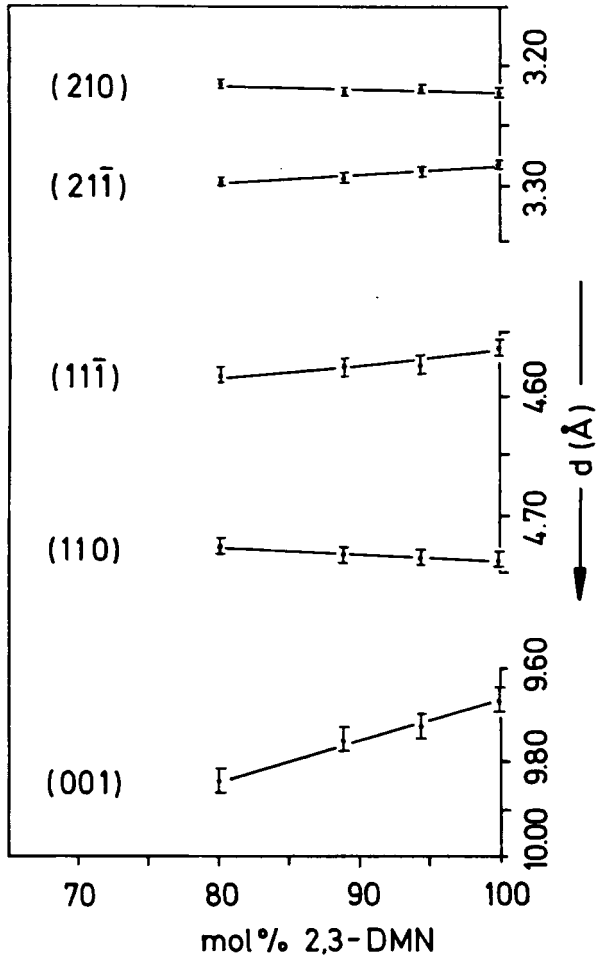

FIGURE 5 Selected lattice parameters in mixed crystals of 2,3-DMN (anthracene) as a function of concentration.

voids which suck-in melt from the solid-liquid boundary layer; this process results in part of the volume being filled for a second time with material, the composition of which is different, in general, from the material that had solidified first. This problem has been treated analytically;[26] here we follow the notation of ref.[21] The accompanying small volume change in the liquid phase is neglected. As is usually done, equal density is assumed for the liquid and solid phases.§

§Including these effects neither principally modifies the basic concept nor substantially alters the results.

In order to be able to interpret the normal freezing results over a wider concentration range and to thus cover a larger portion of the phase diagram, one must take into consideration the possibility of a concentration dependence of the distribution coefficient, $k(c_\ell)$ which requires modification of the normal freezing equation.

The following shows that we can derive the concentration of the corresponding melt, $c_\ell(x)$, for every position x of the phase boundary, from the experimentally determined concentration profile of the first solidified internal main part of the ingot.

Let x′ be a fractional coordinate along the ingot of unit length. With the phase boundary at $x' = x$ the dopant total mass M_ℓ per unit cross section q in the melt is

$$m_\ell = M_\ell/q = c_\ell(x) \cdot (1 - x).$$

After total solidification the main part of this mass is found in the inner portion (of the ingot) which had solidified first; it amounts to

$$m_s^i = \int_x^1 c_s(x')dx'$$

where the subscript s indicates the solid phase, and $c_s(x')$ is the measured distribution function in the internal part of solid ingot. The residual part has solidified later as an outer jacket, as described above. This process occurs rapidly after a crack has formed; consequently, the concentration is that of the *melt* at the phase boundary and no segregation takes place. Therefore,

$$m_s^o = \alpha \int_x^1 c_\ell(x')dx'$$

where α is the product of the (average) fractional volume which is filled for a second time with material and the relative average concentration of this material with respect to the main part of the melt (for the instant when the solid-liquid interface passes the point x). Trivially,

$$m_\ell = m_s^i + m_s^o.$$

or

$$c_\ell(x) \cdot (1 - x) = \int_x^1 c_s(x')dx' + \alpha \int_x^1 c_\ell(x')dx'$$

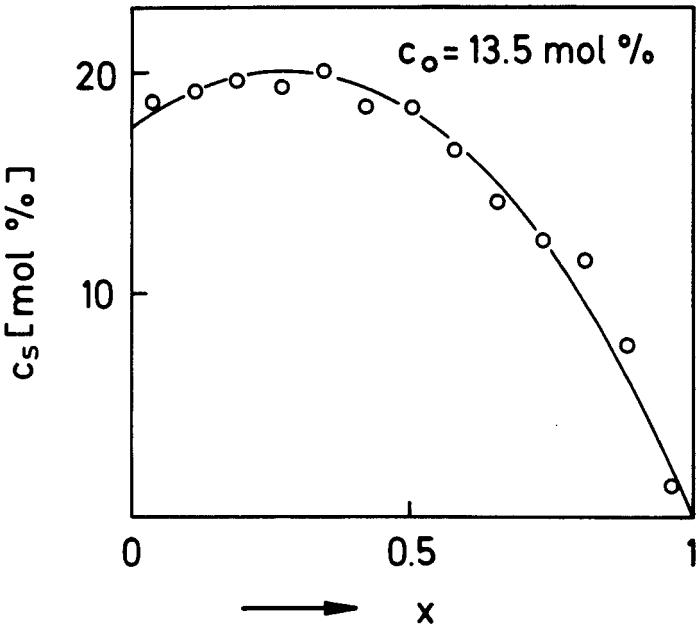

FIGURE 6 Distribution of anthracene in c_o = 13.5 mol-% doped 2,3-DMN after normal freezing, determined by GC analysis (points), and fitted by a second order curve (line) for further analytical evaluation. x is the position on the ingot in fractions of the total ingot length.

The integral equation for $c_\ell(x)$ can be solved approximately numerically after differentation, starting from $x = 0$, where we have $c_\ell(o) = c_o$, which is the initially added concentration. For this purpose the measured $c_s(x)$ distributions were fitted with a second order curve (an example is given in Figure 6); α has to be treated as a free parameter to be varied until conservation of mass is obtained, i.e. until the total mass

$$m = \int_o^1 c_s(x')dx' + \alpha \int_o^1 c_\ell(x')dx'$$

equals the dopant mass which was added

Once knowing $c_\ell(x)$ we can calculate the effective distribution coefficient k_{eff} as a function of c_ℓ which is by definition

$$k_{eff}(c_\ell) = \frac{c_s(x)}{c_\ell(x)}.$$

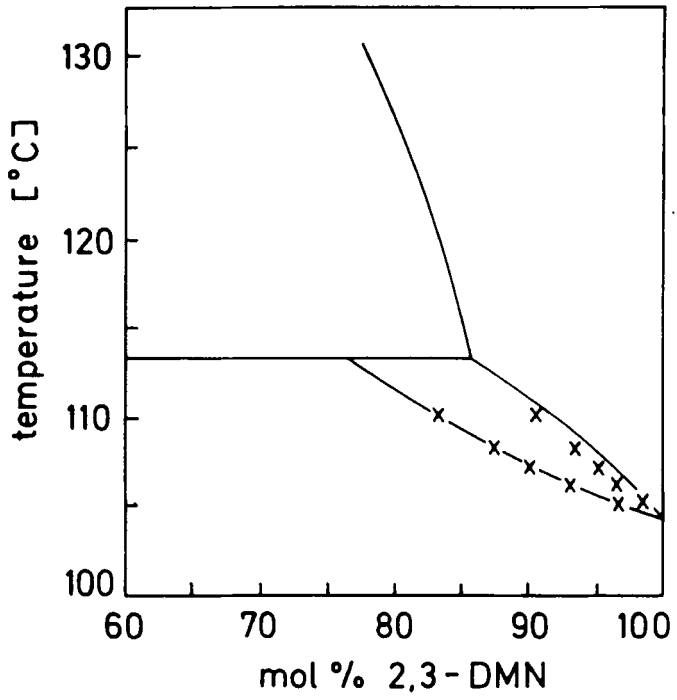

FIGURE 7 Results of normal freezing experiments (×), inserted into the DTA-phase diagram.

Our normal freezing results are drawn as crosses into the initial phase diagram in Figure 7. It appears that the liquidus points from normal freezing nicely parallel the liquidus-curve obtained from DTA. However, they lie systematically slightly lower. This behaviour can be understood on the basis of the Burton-Prim-Slichter theory,[33] which states that, in the kinetically controlled non-equilibrium situation of real crystal growth conditions, a dopant-depleted ($k > 1$) or dopant-enriched ($k < 1$) boundary layer forms at the phase boundary. This is due to preferential incorporation ($k > 1$) or to partial exclusion ($k < 1$) of the dopant according to the segregation coefficient k in conjunction with diffusional limitations of concentration equilization in the melt. The resulting non-equilibrium distribution coefficient k_{eff} is always closer to one than the equilibrium coefficient ($k = 1$ means no segregation at all).

Fortunately, initial supercooling (which cannot easily be avoided completely in a normal freezing experiment) in a $k > 1$ situation does not seriously affect the k-value extrapolated for low concentrations,

$c_l \rightarrow o$. The results with 3 different ingots (doped with c_o = 13.5, 2.9 and 1.5 mol-% anthracene) yielded k ($c_\ell \rightarrow o$) = 2.19, 2.16 and 2.12. The corresponding α values were −0.15, −0.15 and −0.10.

V. PACKING OF THE MIXED CRYSTALS

The change of the lattice parameters of mixed crystals as a function of the anthracene concentration, relative to those of the pure 2,3-DMN, were obtained from the shift of the Guinier reflections, Figure 5, by a least squares fit. The lattice parameters are presented in Table 2 as a function of composition. The strongest dependence (expansion) occurs for the c-axis as reflected by the distance of the (001) lattice planes.

In order to be able to compare the 2,3-DMN crystal structure to that of anthracene, A, we have calculated the projections of the respective unit cells along the intersection line of the molecular planes of the two symmetry-related molecules, Figure 8. The orientations relative to a′ of the traces of the molecular planes in the so defined $a'b$ plane (which are approximately the intermediate molecular axes) are 64.5° and 62.6° for A and 2,3-DMN, respectively, which differ by only 1.9°. The corresponding cross section areas are also very similar: $q_A = a' * b = 46.2$ Å^2 for anthracene and $q_{DMN} = 47.8$ Å^2 for 2,3-DMN. Their relative difference is

$$\frac{q_A - q_{DMN}}{q_A} = -3.5\%.$$

TABLE 2

Variation of the room temperature lattice parameters with concentration for 2,3-DMN(anthracene) mixed crystals compared with the lattice parameters of the neat anthracene crystal.[40] The error of the lattice constants is approximately ±0.01 Å for a, b, c, ±0.1° for β, and ±2 Å^3 for the unit cell volume, V.

mol % 2,3-DMN		100.0	94.5	89.0	80.2	0.0
a	(Å)	7.916	7.915	7.917	7.915	8.561
b	(Å)	6.053	6.052	6.052	6.046	6.036
c	(Å)	10.018	10.086	10.138	10.248	11.163
β	(°)	105.43	105.58	105.86	106.31	124.70
V_o	(Å^3)	462.6	465.3	467.3	470.7	474.2

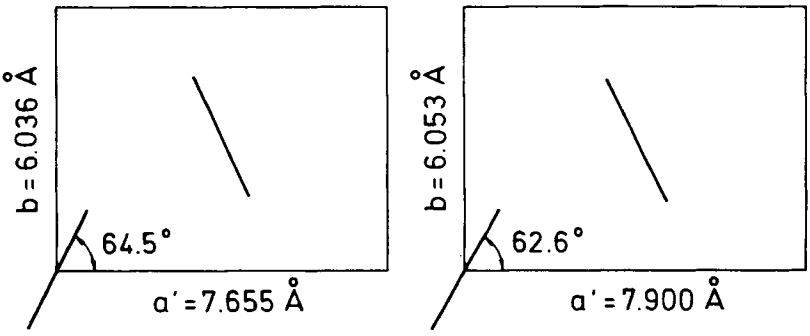

FIGURE 8 Projection of the unit cell of anthracene (left) and 2,3-dimethylnaphthalene (right) along the intersection line of the two symmetry-related molecules.

Thus, in 2,3-DMN the molecular packing in a plane approximately perpendicular to the long molecular axis is less dense than in anthracene. This effect could be due at least partly to some intermolecular steric hindrance caused by the methyl groups.

Orthogonal pseudo- unit cells with these $a'b$-basal planes require for the perpendicular distance $c' \| (a' * b)$, $c'_A = 10.26$ Å for the anthracene structure and $c'_{DMN} = 9.68$ Å for that of 2,3-DMN.

The c' length of the resultant pseudo cell is 5.7% greater for A than for 2,3-DMN,

$$\Delta c' = \frac{c'_A - c'_{DMN}}{c'_A} = 5.7\%.$$

whereas the molecular length of A is 8.4 % greater than that of 2,3-DMN

$$\Delta L = \frac{L_A - L_{DMN}}{L_A} = 8.4\%.$$

(taking $L_A = 11{,}3$ Å and $L_{DMN} = 10{,}4$ Å for the van der Waals length; these values were calculated from the nuclear separations and reasonable hydrogen-carbon bondlengths (1.06 Å for C—H and 1.09 Å for —CH_2—H) and hydrogen van der Waals radii (1.2 Å)).

These calculations indicate that 2,3-DMN is also less densely packed than anthracene in the direction of the long molecular axis.

Finally we also examine the packing problem in the framework of packing coefficients η_i (introduced by reference [34]), defined as the

ratio of the total volume which is occupied by Z molecules of kind i in the unit cell, to that of the entire (empty) unit cell, $V_{o,i}$

$$\eta_i = \frac{Z_i V_i}{V_{o,i}}$$

With $V_A = 171$ Å^3 and $V_{DMN} = 160$ Å^3 calculated with the data of reference [34] and $V_{o,A} = 474.2$ Å^3[40] we obtain $\eta_A = 0.72$ and $\eta_{DMN} = 0.69$, and $\Delta\eta = (\eta_A - \eta_{DMN})/\eta_A = 4\%$, which indicates again that anthracene is more densely packed.

These aspects of the crystal packing density are consistent with the dipolar disorder in the 2,3-DMN lattice, revealed by the X-ray analysis based on the limited data obtainable from the single crystals. It is obvious that disorder prevents molecules from optimally filling the available space. For instance 2,3-DMN (001)-lattice planes with dipolar disorder of the molecules exhibit nonperiodically uneven surfaces. Stacking of these planes necessarily leads to greater distances d_{001} since elevations and depressions are no longer arranged in a complementary periodic sequence.

The question arises: can the loss of van der Waals lattice binding enthalpy, caused by increased distances, be compensated by the dipolar disorder found, so as to render the lattice free energy a minimum and make the disordered configuration a thermodynamically stable one. Most likely the entropy gained by disorder is sufficient to account for the ΔH loss. One might speculate that in certain temperature intervals there is also an ordered "antiferroelectric" phase possible with pairwise antiparallel dipoles whose smaller entropy is compensated by closer c′ packing. The activation energy for a transition, however, might be unreasonably high. An alternative "pyroelectric" ordering with all dipoles parallel appears sterically and electrostatically less favourable.

In this connection and to understand the cause for the observed broad fluorescence lines (see below), it would be highly desirable to learn something about the *microscopic* dipolar packing *correlations* in the disordered phase. Given one molecule at site $\left[\frac{x}{a}, \frac{y}{b}, \frac{z}{c}\right]$ (with relative coordinates $\left[\frac{x_i}{a}, \frac{y_i}{b}, \frac{z_i}{c}\right)$ of the atoms i) with dipol moment "up," the probabilities for finding another one e.g. at site $[\frac{x}{a} + \frac{1}{2} + m, -\frac{y}{b} + \frac{1}{2} + n, \frac{z}{c} + p]$, (m,n,p = 0, ±1, ±2 . . .), with dipol-

moment "up" (w^+) or down (w^-) need not be $w^+ = w^- = 0.5$. In addition to nearest neighbor correlations, there may exist longer range many-particle correlations. Application of methods which probe detailed microscopic structure, such as ESR, NMR, high resolution optical spectroscopy and diffuse X-ray scattering is required to clarify this very interesting point.

Another question is why anthracene is so readily accepted by the 2,3-DMN-lattice. Since packing in a a'b-plane (approximately perpendicular to the long molecular axes) was found to be more or less the same in A and 2,3-DMN, the question reduces to the differences in the c' direction: The incorporation of the longer anthracene molecule is favoured by the fact that disorder in the 2,3-DMN lattice leads to less tight packing in this direction and hence to a larger c' lattice plane distance than that expected for a hypothetical ordered 2,3-DMN structure. In addition, with respect to Figure 2, it is understandable that additional room needed for the ends of anthracene molecules protruding from a molecular (001) layer can be provided for easily by a suitable arrangement (concerning their dipolar orientations) of the 2,3-DMN neighbours of the adjacent layers. Disorder allows this degree of freedom.

Another interesting feature of the mixed crystal formation of 2,3-DMN with anthracene is that admixture of anthracene decreases the average packing coefficient $\bar{\eta}$ of the mixed crystals even though anthracene itself has a higher packing density than 2,3-DMN. This feature makes the existence of an upper miscibility limit understandable. The 2,3-DMN-rich side of the binary system is governed by the framework of the 2,3-DMN lattice which dominates the influence of anthracene with respect to packing forces. The average packing coefficient of a mixed crystal of relative molar concentrations x_i of the components i has been defined as $\bar{\eta} = \Sigma_i x_i \eta_i$, where coefficients η_i calculated for the respective true mixed crystal cell volume $V_o(x_i)$ have to be inserted. These considerations are illustrated by Figure 9, which was plotted with the data of Table 2 and the molecular volumes given above. The "ideal linear combination" curve was calculated assuming a linear concentration dependence of V_o, $V_o(x_i) = \Sigma_i x_i \cdot V_{o,i}$.

VI. FLUORESCENCE SPECTRA OF THE MIXED CRYSTALS

We present only briefly some initial anthracene fluorescence spectra of the system 2,3-DMN (anthracene). Spectra obtained at ~1.7 K for anthracene concentrations 0.3, 1.3, 1.7, and 18.5 mol% are as-

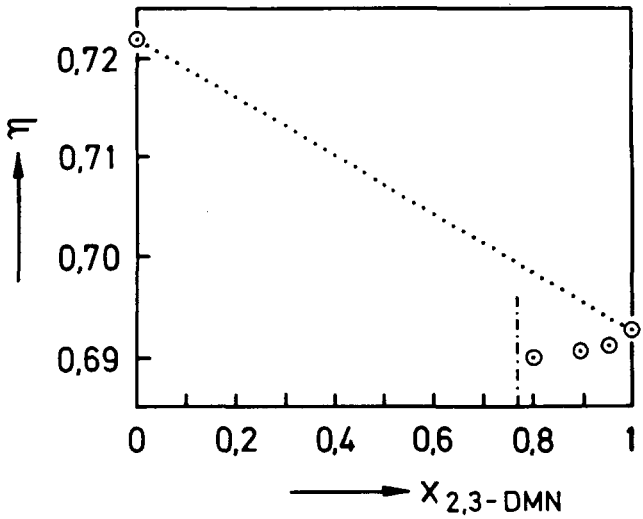

FIGURE 9 Concentration dependence of the average packing coefficient $\bar{\eta}$ (as defined in the text), for the 2,3-DMN (anthracene) mixed crystals. These data are compared with the (hypothetical) concentration dependence of the packing coefficient for the ideal linear combination (dotted) where the mixed crystal unit-cell volume is assumed to increase (or decrease) linearly with the mole fraction.

sembled in Figure 10. For comparison and spectral assignment we also measured an absorption and an emission spectrum for lower anthracene concentration, Figure 11, ($\leq$0.1% for the emission spectrum, 0.12% for the absorption spectrum). The peak positions and a vibrational analysis of the spectra Figure 11 are listed in Table 3.

The following observations were made:

1. The anthracene (guest) fluorescence appears in comparatively broad lines (FWHM 200-300 cm^{-1}), even at liq. He temperature, a surprising result which was (qualitatively) reported before for spectra measured at 35 K.[36] (In other matrices the low temperature anthracene fluorescence can exhibit much sharper lines; the same holds true for neat anthracene crystals.[37]) Considering the dipolar disorder found in the crystal structure determination, we conclude that the main part of this considerable linewidth stems from spatial fluctuations of the site energy (inhomogeneous broadening due to a Gauss distribution of the solvent shift). This conclusion is supported by the fact that the 2,3-DMN host fluorescence lines also remain comparatively broad on cooling (FWHM 100 cm^{-1} at 4.2 K; the origin lies at 30339 cm^{-1}.)[35]

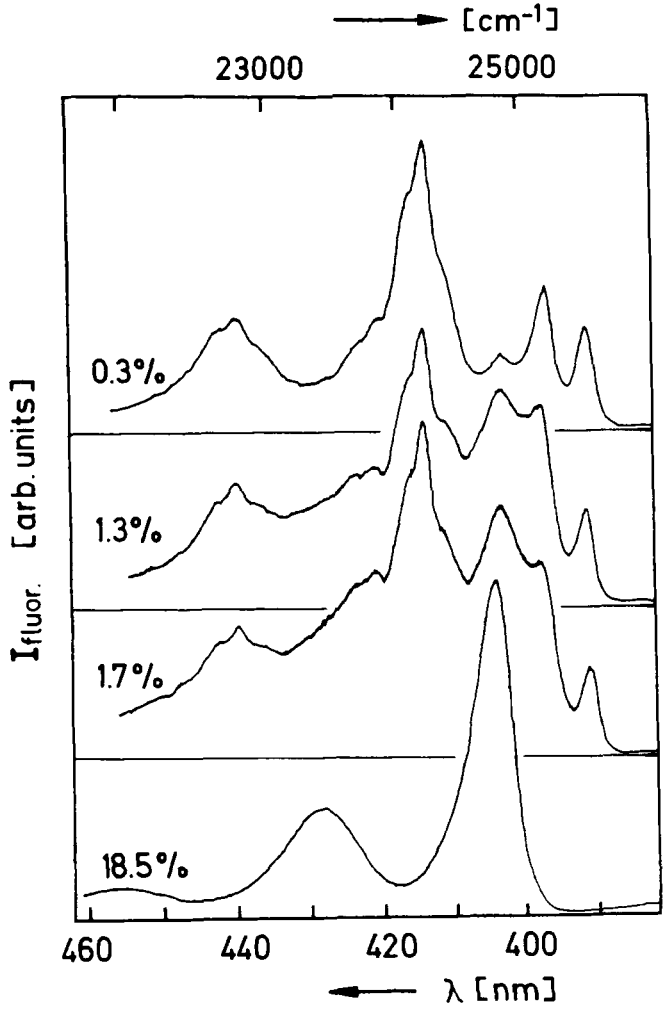

FIGURE 10 Fluorescence spectra at ~ 1.7 K of 2,3-DMN (anthracene) mixed crystals for different anthracene concentrations.

2. The peak positions of the ≤0.1 mol% anthracene emission spectrum, taken at 4.2 K (Figure 11), and of the 0.3, 1.3 and 1.7 % spectra, taken at 1.7 K (Figure 10), are the same within experimental error. However, peak positions previously reported in the literature for 35 K[36] were found at somewhat higher energies ($\Delta\tilde{\nu} \sim 200\ \mathrm{cm}^{-1}$); this shift is too large to be ascribable to the temperature difference alone. The origin of this discrepancy remains unclear, but it is worth

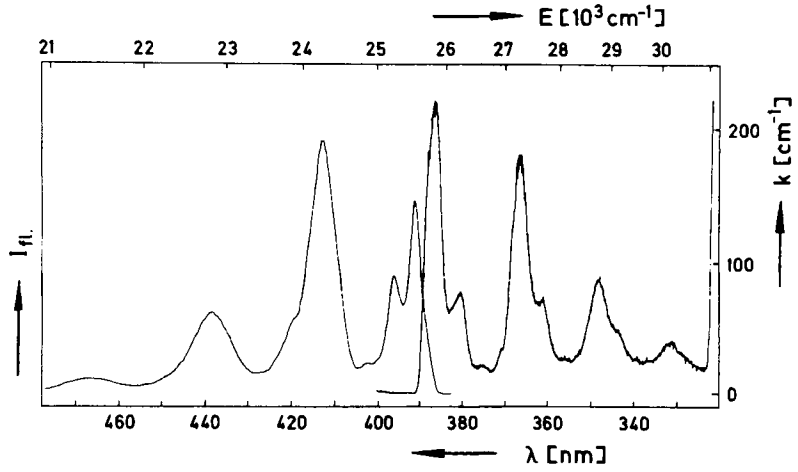

FIGURE 11 Fluorescence and a-polarized absorption spectrum at 4.2 and ~5 K, respectively, of dilute 2,3-DMN (anthracene) mixed crystals with an anthracene concentration of $\leq 10^{-3}$ mol/mol and $1.2 \cdot 10^{-3}$ mol/mol, respectively.

mentioning that the 35 K peak positions reported in this reference essentially agree with our *room temperature* fluorescence peaks; in addition, laser emission from 0.1 mol% anthracene-doped crystals was obtained in the maximum of the 00 + 1432 cm^{-1} fluorescence band at 24400 cm^{-1} at room temperature[20] (and at 24250 cm^{-1} at 5 K.)[46]

3. An analysis of the peak energies of the absorption spectrum (Table 3) yields the well known vibrational progression of the anthracene molecule. The peaks of the fluorescence spectrum can be assigned (within the experimental resolution) to the same vibrational progression if we take into account that the highest energy peak is partly reabsorbed, as is obvious from Figure 11. The origin inferred from the fluorescence progression, $\tilde{\nu} = 25656$ cm^{-1}, is located at lower energy than that of the absorption, $\tilde{\nu} = 25854$ cm^{-1}; the difference amounts to ~ 200 cm^{-1}. The origin of this relaxation shift is presently unknown. Spectral diffusion to lower lying states of an inhomogeneous distribution (although unlikely for the concentration used here),[19] could be one possible reason, energy dissipation by relaxation in the local excited state would be an alternative explanation, while strong electron phonon coupling, transferring the main intensity to the phonon side bands, constitutes a third possibility, which appears very likely.

4. With increasing anthracene concentration a decrease of the rel-

TABLE 3

Energetic postion at liq. He temperature and vibrational analysis of maxima (underlined) and shoulders in the absorption and fluorescence emission spectrum of ~0.1 mol-% anthracene in 2,3-dimethylnaphthalene crystals. The $\Delta\bar{\nu}$ values and the assignment of the emission peaks are based on the assumption that the highest energy fluorescence peak at 25542 cm^{-1}, which is affected by reabsorption, has its true maximum at 25656 cm^{-1}; this extrapolation was made by an average fit of the vibrational progression with the $\Delta\bar{\nu}$ progression of the absorption spectrum. The errors of the absolute energy of the stronger peaks amount to approximately ± 7 cm^{-1}, those of the weaker peaks and shoulders to approximately ± 15 cm^{-1}.

The spectral resolution for the fluorescence spectrum was 12 cm^{-1} (FWHM of calibration lines).

0.12 mol-% A in 2,3-DMN, T~5 K			≤0.1 mol-% A in 2,3-DMN, T = 4.2 K		
absorption			emission		
$\bar{\nu}$[cm^{-1}]	$\Delta\bar{\nu}$[cm^{-1}][a]	assignment	$\bar{\nu}$[cm^{-1}]	$\Delta\bar{\nu}$[cm^{-1}][b]	assignment
<u>25854</u>	0		<u>25542</u>	(reabs.)[c]	(reabs.)[c]
26288	434	434	25246	410	410
26653	799	799	24838	818	818
<u>27285</u>	1431	1431	<u>24224</u>	1432	1432
27709	1855	1431 + 434 (−10)	23803[d]	1853	1432 + 410 (+11)
<u>28701</u>	2847	2 × 1431 (−15)	<u>22825</u>	2831	2 × 1432 (−33)
29109[d]	3255	2 × 1431 + 434 (−41)	—	—	—
<u>30163</u>	4309	3 × 1431 (+16)	<u>21348</u>	4308	3 × 1432 (+12)

[a]differences to the 25854 cm^{-1} maximum
[b]differences to 25656 cm^{-1}
[c]peak shifted to smaller energy due to reabsorption
[d]shoulder

ative fluorescence intensity (with respect to the lower energy peaks) of the highest energy fluorescence peak is observed which can be attributed to progressively stronger reabsorption.

5. With increasing anthracene concentration a peak at 24838 cm^{-1} (402.5 nm) grows relative to the other fluorescence peaks.

6. There is a broad background which increases with rising anthracene concentration until at about 4 mol% anthracene (not displayed in Figure 10) the spectral features change qualitatively in a rather abrupt manner:

7. Above ~ 4 mol% anthracene the maximum of the previous 24838 cm^{-1} peak (which displayed a relative increase with rising anthracene concentration) becomes dominant. It begins to shift slightly and finally settles at 24740 cm^{-1} (404.1 nm) for an anthracene concentration of 18.5 mol%. Two further vibrational satellites, not clearly discernible before, appear at 23540 cm^{-1} (424.7 nm), and at 22211

cm^{-1} (450.1 nm). They shift with increasing anthracene concentration and reach 23346 cm^{-1} (427.9 nm), and 21977 cm^{-1} (454.9 nm), respectively. Their distance from $\tilde{\nu}$ = 24740 cm^{-1} is 1367 and 2 × 1382 cm^{-1}. The final 18.5 mol% anthracene guest fluorescence spectrum resembles that of the neat anthracene crystal, except for the fact that it is composed of much broader lines and has, therefore, less structure, and that its peaks are red-shifted by about 300 cm^{-1}, as can be seen from the comparative common plot, Figure 12.

In what follows we try to give a qualitative explanation of the effects observed at anthracene concentrations above the threshold (~4%) below which the peak positions remain essentially unaltered.

We first present arguments which exclude the possibility that the observed spectra reflect an emission originating from segregations or precipitates of amorphous or crystalline anthracene: Anthracene layers deposited on purpose in an amorphous state (by fast condensation of anthracene vapor onto an 80 K cold substrate) emit a completely different spectrum which consists of only one very broad, unstructured band, peaking at 21000 cm^{-1}.[38] Conversely, even tiny anthracene crystallites emit a spectrum which is composed of narrow lines

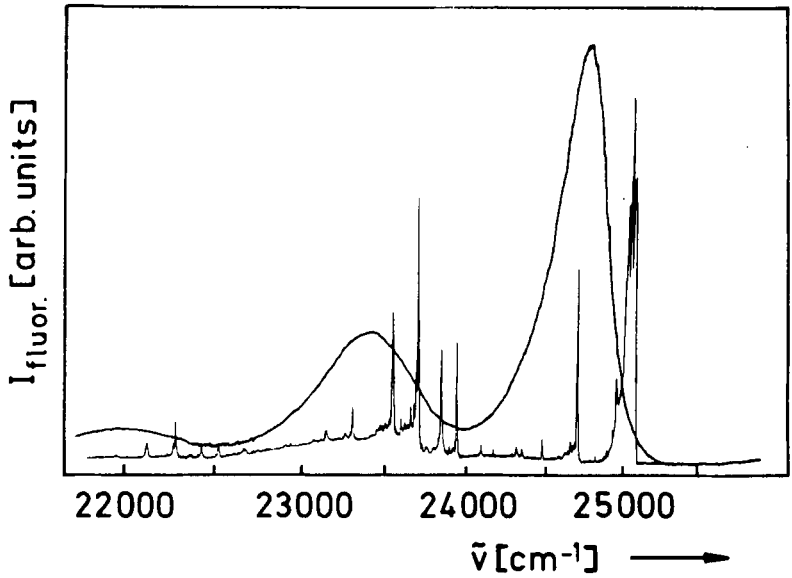

FIGURE 12 Comparison of the ~ 1.7 K anthracene fluorescence spectrum at c = 18.5 mol-%, and the 4.2 K fluorescence spectrum of neat anthracene[37] (narrow spectral lines).

and resembles the one underlaid in Figure 12 (which was obtained for very thin (~1 μm) sublimation flakes.[37]

Next, the fact shall be considered that with rising guest concentration new fluorescence lines emerge and gradually shift to lower energies. We conclude that the only explanation which seems appropriate is that the higher concentration spectra reflect guest–guest interactions. With rising guest concentration guest–guest interactions give rise to new lines originating from pairs, trimers and higher aggregates whose probability distribution function integrally increases and displays a maximum which gradual moves towards the higher aggregates. The probability of finding isolated (noninteracting) monomers drops steeply and, hence, monomeric emission dies out. It is well understood that interacting molecules can emit at lower energies than their matrix-isolated monomers, because the (resonant) interactions shift and split their initially degenerate energy levels.

The additional possibility of transfer of the excitation energy of residual monomers to interacting pairs, trimers etc. by a Förster mechanism or by reabsorption can give a further contribution to the rather sudden decline of the observed monomer emission with increasing concentration and to the bathochromic shift.

In view of the broad spectral bands, however, a distinction of separate monomer, dimer, trimer, etc. lines (observed in other systems)[8] seems impossible in these spectra.

There are two other interesting features which require an interpretation, namely that the (low temperature) fluorescence bands remain broad even at the highest anthracene concentrations (e.g. at 18.5 mole%, Figure 10), and that the centers of gravity of these vibrational bands lie at lower energies than the corresponding (sharp) lines of the neat anthracene crystal, Figure 12.

The comparatively sharp low temperature fluorescence lines of the neat anthracene crystal have been interpreted in terms of transitions from near the lower band edge of an excitonic band of width 403 cm^{-1}.[47] Small, irregular clusters and disorder of the 2,3-DMN host crystal preclude a description of the excited guest states in terms of a band model. Emission from the entire range of split levels may occur. Since the width of the split level distribution is essentially caused by the nearest neighbour interactions, it is not very different for the cluster and for the band situation. Enhanced electron–phonon coupling in the situation of local clusters in disordered surroundings may also contribute to an increase of the linewidth.

A bathochromic shift of the entire anthracene guest fluorescence

spectrum—at high guest concentrations—to even lower energies than those of the neat anthracene crystal can have several causes: I) Strong electron-phonon coupling can transfer the main intensity of each of the vibronic transitions to (lower energy) phonon side bands. II) Stronger anthracene-anthracene interactions in the 2,3-DMN lattice, resulting from the slightly smaller unit cell of the mixed crystals compared to the neat anthracene crystal (Table 2), and from the more perpendicular orientations of the long molecular axes relative to the (001) cleavage plane in the mixed crystal (yielding closer approach of the anthracene molecular centers of accidentally neighbouring guest molecules in the individual 2,3-DMN (001) layers, and concomitantly, closer interactions of the π-electrons, in the simplest way of looking at it). A red shift of $\sim 300\ cm^{-1}$ is obviously too large to be accounted for fully by cause I) alone.

A third possibility, a stronger site shift interaction of the anthracene molecules with the 2,3-DMN molecules than among themselves is ruled out by comparing the singlet S_1 energy of a fictive isolated anthracene molecule in the anthracene crystal, $\tilde{\nu}_{IMC} = 25301(42)\ cm^{-1}$ [48] and the higher energy of the extrapolated "origin" (maximum) of the (dilute) anthracene guest fluorescence in 2,3-DMN, $\tilde{\nu} = 25656\ cm^{-1}$ (Table 3)—irrespective of whatever the true nature of this peak is (maximum of inhomogeneously broadened 0-0 transition, phonon side band, etc.).

Our present knowledge of the 2,3-DMN(A) system is insufficient for deriving a detailed understanding of the pronounced spectral changes of the anthracene fluorescence emission which occur with increasing anthracene concentrations. Time-resolved spectroscopy, site selection spectroscopy, and optical hole burning experiments may help to further elucidate the molecular interactions and the pathways of energy transfer, and to establish if it can be described as impurity band conduction.[4,41,42]

In summary, we have studied the crystal structure of 2,3-dimethylnaphthalene and the 2,3-dimethylnapthalene-rich part of the binary phase diagram with anthracene, where mixed crystals form with anthracene concentrations up to 23 mol%. The anthracene fluorescence-emission at low concentrations occurs in a vibrational progression consisting of fairly broad lines which are believed to reflect the disordered 2,3-dimethylnaphthalene lattice. Above ~4 mol% anthracene the fluorescence spectra are dominated by emission from interacting anthracene guest molecules which give rise to a considerable red shift.

Acknowledgments

We wish to express our gratitude to Prof. H. Bässler, Dr. H. Port and Prof. H. C. Wolf for helpful discussions, and to Prof. K. Walenta, Institut für Mineralogie und Kristallchemie of the University of Stuttgart for allowing us to use their DTA equipment. Valuable assistance with the crystal structure determination by E. Eckle and K. Jogun is greatly appreciated. The fluorescence spectrum in Figure 11 was kindly measured by Mrs. Dr. A. Hammer. Thanks are also due to M. Gerdon and Ch. Herb for their assistance with zone refining, normal freezing and crystal growth. Mrs. G. Pampel did careful gas chromatographic analyses.

This work was partly supported by the Stiftung Volkswagenwerk.

References

1. H. C. Wolf in: P. Reineker, H. Haken and H. C. Wolf eds. "Organic Molecular Aggregates," p. 2 (Springer Verlag, Berlin, 1983).
2. M. Pope and C. E. Swenberg, "Electronic Processes in Organic Crystals," (Clarendon Press, Oxford University Press, New York 1982).
3. V. M. Agranovich and M. D. Galanin, "Electronic Excitation Energy Transfer in Condensed Matter," (North Holland Publ. Comp., Amsterdam 1982).
4. A. H. Francis and R. Kopelman, "Excitation Dynamics in Molecular Solids," in: "Laser Spectroscopy of Solids," W. M. Yen, and P. M. Selzer eds., p. 241, (Springer Verlag, Berlin 1981).
5. V. M. Kenkre and P. Reineker, "Exciton Dynamics in Molecular Crystals and Aggregates," (Springer Verlag, Berlin 1982).
6. P. Reineker, H. Haken, and H. C. Wolf eds.; "Organic Molecular Aggregates," (Springer Verlag, Berlin 1983).
7. G. G. Roberts, N. Aspley and R. W. Munn, "Temperature-Dependent Electronic Conduction in Semiconductors," *Physics Reports*, **60**, 59 (1980); R. W. Munn, *Inst. Phys. Conference Ser.*, **58**, p. 98 (Physics of Dielectrics, Canterbury 1980).
8. (b): S. D. Colson, S. M. George, T. Keyes and V. Vaida, *J. Chem. Phys.*, **67**, 4941 (1977); (n): M. Schwörer and H. C. Wolf, *Mol. Cryst.*, **3**, 177 (1967); D. M. Hanson, *J. Chem. Phys.*, **52**, 3409 (1970); H. K. Hong and G. W. Robinson, *J. Chem. Phys.*, **54**, 1369 (1971); H. Hinkel, H. Port, H. Sixl, M. Schwörer, P. Reineker and D. Reinhardt, *Chem. Phys.*, **31**, 101 (1978); E. M. Monberg and R. Kopelman, *Mol. Cryst. Liq. Cryst.*, **57**, 271 (1980); J. P. Lemaistre, A. Blumen, F. Dupuy, Ph. Pee, R. Brown and Ph. Kottis, *J. Phys. Chem.*, **88**, 4655 (1984). (n, a): H. C. Wolf and H. Port in: "Molecular Spectroscopy of Dense Phases," (Elsevier, Amsterdam 1976), p. 31; H. Port in: P. Reineker, H. Haken, and H. C. Wolf eds. "Organic Molecular Aggregates" p. 22 (Springer, Berlin 1983); U. Doberer and H. Port, *Z. Naturforsch.*, **39**, 413 (1984); (d): R. M. Hochstrasser and J. D. Whiteman, *J. Chem. Phys.*, **56**, 5945 (1972); R. Schmidberger, Dissertation, Univ. Stuttgart (1974); (py): K. Mistelberger and H. Port, *Mol. Cryst. Liq. Cryst.*, **57**, 203 (1980); (ph): D. D. Smith, R. D. Mead and A. H. Zewail, *Chem. Phys. Letters*, **50**, 358 (1977); U. Doberer, H. Port and R. Sauter, *Chem. Phys.*, **85**, 431 (1984); (t): S. M. Janes and H. C. Brenner, *Chem. Phys.*, **91**, 449 (1984), and references given therein.
9. A. I. Kitaigorodsky, "Molecular Crystals and Molecules," (Academic Press 1973).
10. V. Vaida and S. D. Colson, *Mol. Phys.*, **35**, 965 (1978); S. D. Colson and M. Okumura, *Mol. Cryst. Liq. Cryst.*, **57**, 255 (1980).
11. D. Schweitzer and H. Zimmermann, *Z. Naturforsch.*, **34a**, 1185 (1979).
12. H. Port, H. Schneckenburger, and H. C. Wolf, *Chem. Phys. Letters*, **61**, 503 (1979); H. Schneckenburger, Diplomarbeit, Univ. Stuttgart (1976).

13. N. Karl, *Chemica Scripta*, **17**, 201 (1981).
14. R. A. M. Scott, S. R. Laridjani and D. J. Morantz, *J. Crystal Growth*, **22**, 53 (1974).
15. N. Karl, M. Warth, and J. J. Stezowski, to be published.
16. N. Karl and Th. Lang, unpublished results.
17. N. Karl, "Halbleitereigenschaften des organischen Molekülkristalls Anthracen" Habilitationsschrift, Universität Stuttgart, 1975.
18. C. Bogus, Dissertation, Universität Giessen (1967); W. -W. Falter, *Z. Naturforsch.*, **31a**, 251 (1976).
19. F. Belitz, *Z. Naturforsch.*, **25a**, 955 (1970).
20. N. Karl, *J. Luminescence*, **12/13**, 851 (1976); idem in: Lasers in Physical Chemistry and Biophysics, p. 61 (Elsevier Sci. Publ. Comp., Amsterdam 1975).
21. N. Karl "High Purity Organic Molecular Crystals," in: Crystals, Vol. 4, p. 7 (Springer Verlag, Berlin 1980).
22. J. Kalus and N. Karl, unpublished results.
23. H. Klapper and N. Karl, 7th Internat. Conf. Crystal Growth Stuttgart, poster (1983).
24. H. Steybe, Ingenieurarbeit, Universität Stuttgart 1969.
25. N. Karl and K.-H. Probst, *Mol. Cryst. Liq. Cryst.*, **11**, 155 (1970).
26. N. Karl and H. Feederle, unpubl. results; cf. H. Feederle, Diplomarbeit, Universität Stuttgart 1974, and N. Karl, ref. 21, p. 34 (cf. p. 15); for the general case of non unity crossection q, the equation in line 26, p. 34 of ref. 21 should read correctly $\bar{\alpha}\, d\, u = \alpha\, q$.
27. A. Gäumann, *Chimia*, **20**, 82 (1966).
28. J. M. Stewart, P. A. Machin, C. S. Dickinson, H. L. Ammon, H. Heck and H. Flack, *The X-ray System, Version 1976* (University of Maryland, Computer Science Center, College Park, MD, Technical Report TR-446 (1976).
29. From the symmetry of the conoscopic interference pattern in monochromatic light, viewed through the cleavage plane, (in confirmation of the results of ref. 30), and from the anisotropy and orientation of the optic tensor (indicatrix), measured by an Abbe refractometer (N. Karl and A. Valera, unpublished results).
30. Z. Tomczak, A. Tramer, J. W. Rohleder, and T. Luty, *Acta Physica Polonica*, **32**, 731 (1967).
31. Temperature-dependent Guinier photographs were kindly taken for us by A. Simon and W. Rötenbach at the Max-Planck-Institute für Festkörperforschung, Stuttgart.
32. A. R. McGhie and G. J. Sloan, 5th Molecular Crystal Symposium, Philadelphia 1970, Abstract Book p. 109.
33. I. A. Burton, R. C. Prim, and W. P. Slichter, *J. Chem. Phys.*, **21**, 1987 (1953).
34. A. I. Kitaigorodsky, "Organic Chemical Crystallography," Consultants Bureau, New York 1961.
35. P. Niedermann, Diplomarbeit, Universität Stuttgart 1970.
36. R. Legler, *Z. Naturforsch.*, **26a**, 988 (1971).
37. E. Glockner and H. C. Wolf, *Z. Naturforsch.*, **24a**, 943 (1969).
38. J. Hofmann, K. P. Seefeld, W. Hofberger, and H. Bässler, *Mol. Phys.*, **37**, 973 (1979).
39. V. I. Ponomarev, *Sov. Phys. Cryst.*, **21**, 215 (1976).
40. A. Mathieson, J. M. Robertson and V. C. Sinclair, *Acta Cryst.*, **3**, 245 (1950); V. C. Sinclair, J. M. Robertson, and A. McL. Mathieson, *Acta Cryst.*, **3**, 251 (1950).
41. J. Klafter and J. Jortner, *J. Chem. Phys.*, **71**, 2210 (1979).
42. R. F. Loring, H. C. Andersen and M. D. Fayer, *Chem. Phys.*, **70**, 139 (1982); R. F. Loring and M. D. Fayer, *J. Chem. Phys.*, **76**, 2015 (1982).
43. Program JIMPLAN, an Oblique Plane Fourier Plotting Program, in which the slant-plane Fourier transform routine of B. M. van de Waal has been incorporated by N. K. Hanson.